The Astrophysical Journal, 888:122 (15pp), 2020 January 10 https://doi.org/10.3847/1538-4357/ab5f07

O_2- and CO-rich Atmospheres for Potentially Habitable Environments on TRAPPIST-1 Planets

Renyu Hu[1,2], Luke Peterson[1,3], and Eric T. Wolf[4]
[1] Jet Propulsion Laboratory, California Institute of Technology, Pasadena, CA 91109, USA; renyu.hu@jpl.nasa.gov
[2] Division of Geological and Planetary Sciences, California Institute of Technology, Pasadena, CA 91125, USA
[3] Northwestern University, Evanston, IL 60201, USA
[4] Laboratory for Atmospheric and Space Physics, Department of Atmospheric and Oceanic Sciences, University of Colorado, Boulder, CO 80303, USA
Received 2019 July 2; revised 2019 August 19; accepted 2019 December 3; published 2020 January 16

Abstract

Small exoplanets of nearby M-dwarf stars present the possibility of finding and characterizing habitable worlds within the next decade. TRAPPIST-1, an ultracool M-dwarf star, was recently found to have seven Earth-sized planets of predominantly rocky composition. The planets e, f, and g could have a liquid water ocean on their surface given appropriate atmospheres of N_2 and CO_2. In particular, climate models have shown that the planets e and f can sustain a global liquid water ocean, for $\geqslant$0.2 bar CO_2 plus 1 bar N_2, or $\geqslant$2 bar CO_2, respectively. These atmospheres are irradiated by ultraviolet emission from the star's moderately active chromosphere, and the consequence of this irradiation is unknown. Here we show that chemical reactions driven by the irradiation produce and maintain more than 0.2 bar O_2 and 0.05 bar CO if the CO_2 is $\geqslant$0.1 bar. The abundance of O_2 and CO can rise to more than 1 bar under certain boundary conditions. Because of this O_2–CO runaway, habitable environments on the TRAPPIST-1 planets entail an O_2- and CO-rich atmosphere with coexisting O_3. The only process that would prevent runaway is direct recombination of O_2 and CO in the ocean, a reaction that is facilitated biologically. Our results indicate that O_2, O_3, and CO should be considered together with CO_2 as the primary molecules in the search for atmospheric signatures from temperate and rocky planets of TRAPPIST-1 and other M-dwarf stars.

Unified Astronomy Thesaurus concepts: Extrasolar rocky planets (511); Habitable planets (695); Super Earths (1655); Habitable zone (696); Exoplanet atmospheres (487); Astrobiology (74)

1. Introduction

The era of characterizing temperate and rocky exoplanets has begun. Ground-based surveys have found temperate planets hosted by M-dwarf stars like the TRAPPIST-1 planets and LHS 1140 b (Dittmann et al. 2017; Gillon et al. 2017). The K2 mission and the *Transiting Exoplanet Survey Satellite* (*TESS*) are finding a few tens transiting and temperate planets around nearby M stars (e.g., Sullivan et al. 2015). Orbiting small stars, these planets provide an accelerated path toward finding and characterizing potentially habitable worlds. The TRAPPIST-1 planets already have transmission spectra measured by *Hubble* (De Wit et al. 2018; Zhang et al. 2018). With >7 times more collecting area and infrared instruments, the *James Webb Space Telescope* (*JWST*) will be capable of providing a more detailed look into the atmosphere of these cold exoplanets (Beichman et al. 2014).

A key factor that impacts the atmospheric compositions of rocky planets around M-dwarf stars is stellar ultraviolet (UV) irradiation. UV radiation dissociates CO_2 into CO and O, but the direct recombination of the two products is slow. Two O produced then combine to form O_2. In the solar system, the CO_2 atmosphere of Mars is stabilized principally by catalytical cycles of OH and HO_2 that recombine CO and O_2 (McElroy & Donahue 1972; Nair et al. 1994), while that of Venus is additionally stabilized by chlorine species (McElroy et al. 1973). If the star is an M dwarf, its irradiation is strong in the far-UV (FUV) bandpass but weak in the near-UV (NUV) bandpass (France et al. 2013). Because FUV radiation dissociates CO_2, and NUV radiation amplifies the catalytical cycles of OH and HO_2, a liquid-water-ocean planet of an M dwarf is inclined to accumulate CO and O_2 in the atmosphere. Using the spectrum of the M dwarf GJ 876, atmospheric photochemistry models have predicted an O_2 mixing ratio up to 5% in an N_2-dominated atmosphere with 0.05 bar CO_2 (Domagal-Goldman et al. 2014; Tian et al. 2014; Harman et al. 2015). Atmospheric photochemistry models have also shown that massive O_2 and CO would be produced from CO_2-dominated atmospheres of desiccated—and hence uninhabitable—rocky planets of M-dwarf stars (Gao et al. 2015).

Climate models of the planets TRAPPIST-1 e, f, and g indicate that they need more than 0.05 bar CO_2 to sustain a global liquid water ocean, because the planets have lost their primordial hydrogen envelopes due to X-ray and extreme-UV irradiation (Bolmont et al. 2017; Bourrier et al. 2017). For an atmosphere with 1 bar N_2 and varied abundance of CO_2 on planet e, ice would cover 57% of the planet at 0.1 bar CO_2, and the coverage drops quickly to nearly zero at $\geqslant$ 0.2 bar CO_2 (Wolf 2017). On the planet f, $\geqslant$ 2 bar CO_2 are required (Wolf 2017; Turbet et al. 2018). Substituting CO_2 with CH_4 or NH_3 as the main greenhouse gas would be unlikely to sustain the habitability, because of their much weaker greenhouse effect and tendency to form photochemical hazes that cause an anti-greenhouse effect (Turbet et al. 2018). The photochemical lifetime of CH_4 could however be quite long on TRAPPIST-1 planets for weaker NUV radiation (e.g., Rugheimer et al. 2015).

To investigate the effect of stellar irradiation on this high CO_2 abundance, we use our photochemistry model (Hu et al. 2012, 2013) to determine the steady-state composition of the atmospheres under irradiation. The photochemistry model uses the atmospheric pressure–temperature profiles generated by the

3D climate model (Wolf 2017), which was calculated for varied partial pressures of CO_2. We find that more than 0.2 bar O_2 and 0.05 bar CO are produced in the steady state if the CO_2 partial pressure is $\geqslant$0.1 bar. The abundance of O_2 and CO can rise to more than 1 bar depending on their deposition velocities, which constitutes an "O_2–CO runaway." The paper is organized as follows. We describe our models, including the 3D climate model in Section 2, present the conditions and the chemistry of the O_2–CO runaway in Section 3, discuss its climate implications, feedback, and geologic context in Section 4, and conclude in Section 5.

2. Methods

2.1. Photochemistry Model

The photochemistry model used in this study (Hu et al. 2012, 2013) has been validated by computing the atmospheric compositions of present-day Earth and Mars, as the outputs agreed with the observations of major trace gases in Earth's and Mars' atmospheres. The model has also been used to determine the photochemical oxygen buildup in abiotic atmospheres (Hu et al. 2012; James & Hu 2018). For the latter purpose, the model has been compared with other photochemistry models in detail, and we have found good agreement (Gao et al. 2015; Harman et al. 2018). The photochemistry model solves the one-dimensional chemical transport equation for 111 O, H, C, N, and S species including sulfur and sulfuric acid aerosols. The full species and reaction list can be found in Hu et al. (2012). The model seeks to balance product and loss terms from all chemical and photochemical reactions for each gas at each altitude level. We typically do not assume photochemical equilibrium for any gas; so, unless otherwise stated, all gases are included in the full chemical transport calculation. The system is considered as converged to a steady state if the minimum variation timescale is greater than, for instance, the age of the solar system (10^{17} s).

In the models that feature the O_2–CO runaway, the ambient pressure changes in the simulation because the produced O_2 and CO meaningfully contribute to the pressure. Our photochemistry model self-consistently calculates the effect of the changing ambient pressure on the kinetic rates. Because the photochemistry model solved the continuity equation of number densities (Hu et al. 2012), the total number density of each layer is obtained by summing the number densities of all molecules in that layer. As such, the total number density, and thus the pressure, of each layer is updated after each time stepping. The changing pressure affects the rates of termolecular reactions, because they are proportional to the total number density, and also affects the rates of photolysis via radiative transfer in the atmosphere. These effects are self-consistently calculated in each time step. In particular, an important termolecular reaction is the direct combination between CO and O in the atmosphere, CO+O+M $\rightarrow$ CO_2+M, and its rate increases with the ambient pressure. This feedback loop eventually limits the size of the atmosphere when the O_2–CO runaway is strong.

We adopt the eddy diffusion coefficient derived from the number density profiles of trace gases on Earth (Massie & Hunten 1981). The eddy diffusion coefficient is characterized by a high value in the convective troposphere, a minimum corresponding to the tropopause, and an increasing value with smaller number densities in the nonconvective stratosphere.

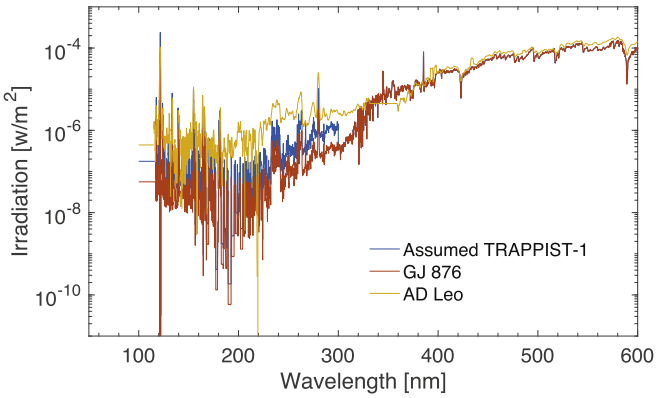

Figure 1. Stellar spectra used in this study. All spectra are scaled by their bolometric luminosity with respect to TRAPPIST-1. The spectrum of GJ 876 is obtained by the MUSCLES project, which uses *Hubble* observations in the UV to reconstruct the intrinsic stellar Lyα emissions (France et al. 2016). The spectrum of TRAPPIST-1 at wavelengths >300 nm is the same as the scaled GJ 876 spectrum, but at wavelengths <300 nm a different scaling according to the measured Lyα flux is applied. The spectrum of AD Leo, a more active M star, is from Segura et al. (2005). The Lyα reconstruction was not performed on the spectrum of AD Leo.

When the ambient pressure increases, the eddy diffusion coefficient as a function of altitude is unchanged. This ensures vigorous transport in the atmosphere and preserves the sensitivity of the eddy diffusion coefficient to the convective nature of the atmosphere. There could be additional effects of the changing pressure on the eddy diffusion coefficient, and we thus caution that the results may be dependent on the assumption of the eddy diffusion.

To simulate the effect of lightning, we adopt the terrestrial production rate of NO from lightning, $6 \times 10^8\,\mathrm{cm^{-2}\,s^{-1}}$(Schumann & Huntrieser 2007), which is already greater than the majority of the parameter space explored previously for N_2–CO_2–H_2O atmospheres (Wong et al. 2017; Harman et al. 2018). In addition, it is found that in an atmosphere O_2 richer than Earth's atmosphere, the NO production rate from lightning can be higher, up to $\sim 10^9\,\mathrm{cm^{-2}\,s^{-1}}$ (Harman et al. 2018). We also consider this higher production rate in a sensitivity study.

The stellar spectrum of TRAPPIST-1 has not been measured in UV. Therefore, we use the UV spectrum of GJ 876 obtained by the MUSCLES project as the proxy (France et al. 2016). The survey uses *Hubble* observations in the UV to reconstruct intrinsic stellar Lyα emissions. The visible spectrum is obtained from ground-based observations, and the infrared spectrum is from the PHOENIX stellar atmosphere models. GJ 876, an M5V star of $T_{\rm eff} \sim 3100$ K, is one of the closest stars to TRAPPIST-1 ($T_{\rm eff} \sim 2600$ K) in the MUSCLES sample. As shown in Figure 1, we scale the spectrum in the UV wavelength (<300 nm) by the measured Lyα flux of TRAPPIST-1 (Bourrier et al. 2017, a factor of 0.135 with respect to GJ 876, Youngblood et al. 2016) and that in the visible wavelength (>300 nm) by the measured bolometric luminosity of TRAPPIST-1 (Van Grootel et al. 2018, a factor of 0.0428 with respect to GJ 876, Von Braun et al. 2014). In addition, we explore in a sensitivity study a spectral shape in the UV as AD Leo, an active M4.5V star. Figure 1 shows that the spectral shape of AD Leo has a larger FUV/NUV ratio, but the FUV flux may be inaccurate as Lyα reconstruction was not performed.

Table 1
Starting Scenarios of This Study and Their Key Climate Characteristics Based on the 3D Model of Wolf (2017)

Planet	N_2	CO_2	*T* Surf Globe (K)	Ice Fraction	Initial Mixing Ratio of H_2O at Surface	Top of Atmosphere Altitude (km)
TRAPPIST-1 e	1 bar	None	227	86%	0.0018	88
TRAPPIST-1 e	1 bar	0.0004 bar	241	80%	0.0037	84
TRAPPIST-1 e	1 bar	0.01 bar	254	73%	0.0056	84
TRAPPIST-1 e	1 bar	0.1 bar	274	57%	0.0138	83
TRAPPIST-1 e	1 bar	0.2 bar	285	18%	0.0213	82
TRAPPIST-1 e	1 bar	0.4 bar	303	0%	0.0407	71
TRAPPIST-1 e	1 bar	1 bar	333	0%	0.1001	73
TRAPPIST-1 f	None	1 bar	227	100%	0.0007	56
TRAPPIST-1 f	None	2 bar	289	2%	0.0067	59
TRAPPIST-1 f	None	5 bar	335	0%	0.0444	66

Last but not least, our model ensures the redox flux balance of the atmosphere and the ocean. The convergence of the photochemistry model itself ensures the balance of the redox budget of the atmosphere. However, this does not ensure that the results are realistic on planets, as there is no known abiotic way to deposit reducing species at the bottom of the ocean. We therefore enforce the balance of the redox budget of the ocean by requiring the net transfer of the redox flux between the atmosphere and the ocean to be zero (Domagal-Goldman et al. 2014; Harman et al. 2015; James & Hu 2018). In practice, this balance is achieved by including a pseudo return flux of hydrogen. If we find a net transfer of the redox flux from the atmosphere to the ocean in a converged solution, we include this net flux as a return flux of hydrogen from the ocean to the atmosphere and relaunch the simulation. We repeat the process until the imbalance is no larger than 1% of the outgassing redox flux. This way, our results satisfy the redox balance for both the atmosphere and the ocean.

2.2. Outgassing and Deposition

We use the volcanic activity rate of present-day Earth and the per-mass outgassing rate calculated for mid-ocean ridge basalts (Gaillard & Scaillet 2014) to calculate the gas outgassing rate. The outgassing rate is $1.5 \times 10^9\,cm^{-2}\,s^{-1}$ for CO, H_2, and SO_2, and $1.5 \times 10^8\,cm^{-2}\,s^{-1}$ for H_2S (see James & Hu 2018 for details). TRAPPIST-1 e may have a tidal heating flux corresponding to 1 to ~10 times the geothermal heat flux (Luger et al. 2017; Papaloizou et al. 2017). We have performed an additional set of simulations assuming a 10 times higher volcanic outgassing rate and found no noticeable difference in the O_2 or CO partial pressure. The model has a full sulfur chemistry network (Hu et al. 2013), and we find that the outgassed H_2S and SO_2 is either rained out directly or oxidized to H_2SO_4. The H_2SO_4 is then rained out. The outgassing rate, even at the 10 times level, is not high enough to produce a H_2SO_4 aerosol layer in the atmosphere.

The standard model assumes a deposition velocity of zero for O_2 and includes a deposition velocity of either zero or 10^{-8} $cm\,s^{-1}$ for CO. The nonzero value for CO comes from assuming the aqueous formation of formate ($CO + OH^- \rightarrow COOH^-$) as the rate-limiting step to remove CO (Kharecha et al. 2005). Other reactions acting as a rate-limiting step would lead to even lower deposition velocities (Harman et al. 2015), and thus the zero value for CO is included as another end-member scenario. We find that the exact abundance of O_2 versus CO in the O_2–CO runaway scenarios is quite sensitive to the choice of deposition velocity of CO (Section 3.1).

In addition to the standard model, we have performed additional simulations to evaluate the effect of potential sinks for O_2 in the ocean. (1) A deposition velocity of $10^{-8}\,cm\,s^{-1}$ for O_2 would be possible for the potential recombination of O_2 and CO in hydrothermal flow through the mid-ocean ridges (Harman et al. 2015). We observed no noticeable changes in the results when adopting this deposition velocity. (2) A second potential sink of O_2 is Fe^{2+} input in the ocean from crust formation. We describe the test to include this sink in Section 3.1. (3) As a limiting scenario, we consider the possibility that direct recombination of O_2 and CO occurs rapidly in the surface ocean. This would enable the rapid deposition of both O_2 and CO, and we also describe its impact on the result in Section 3.1.

For scenarios with substantial O_2 buildup, O_3 has a substantial mixing ratio at the surface and therefore can have a substantial deposition flux onto the surface. This would make the model results sensitive to the choice of the deposition velocity of O_3. Some of the previous studies assume O_3 to be the short-lived species in photochemical equilibrium (Harman et al. 2015, 2018), thus removing the need to specify a deposition velocity. On Earth, the deposition velocity of O_3 is very different between the land and the ocean. As a slightly soluble gas, O_3's deposition velocity over the ocean is limited by the mass transfer rate in the liquid phase (Broecker & Peng 1982). Using the typical mass transfer coefficient and the Henry's law coefficient for O_3, the deposition velocity is approximately $10^{-3}\,cm\,s^{-1}$, and this value is consistent with the measurements over Earth's ocean (Hardacre et al. 2015). The surface resistance of O_3 is considerably smaller over Earth's land, and the measured deposition velocity is typically on the order of $0.3\,cm\,s^{-1}$. While this value is also valid for deserts (Hardacre et al. 2015), the lower resistance is most likely due to the prevalence of biosphere on Earth. We therefore adopt the value of $10^{-3}\,cm\,s^{-1}$ in the standard model and explore a value of $0.1\,cm\,s^{-1}$ in a sensitivity study. The standard value is the same as that used in Tian et al. (2014).

2.3. Climate Modeling and Temperature–Pressure Profiles

To initialize the photochemical model, we use the substellar hemisphere mean vertical profile generated by the 3D climate model (Wolf 2017) in this study. The scenarios used in this study are summarized in Table 1. We fix the number density of water vapor at the bottom of the atmosphere according to the

3D model and allow water vapor to condense out as the temperature drops with altitude. The top of the atmosphere is assumed to be 0.1 Pa, corresponding to the different altitudes between the scenarios due to different temperatures and mean molecular weights. The mass and the radius of each planet are the measured values from Grimm et al. (2018).

When O_2–CO runaway occurs, O_2 and CO contribute meaningfully to the total atmospheric pressure. New for this work, we have conducted several additional 3D climate model simulations to test the climate effects of this increased atmospheric pressure. The radiative effects of O_2 and CO are primarily felt indirectly through their contribution to the total atmospheric pressure and subsequent pressure broadening of CO_2 absorption features, which can have a significant warming effect on climate (Goldblatt et al. 2009). As presently configured, our 3D model handles only N_2, H_2O, and CO_2, and therefore, we have substituted N_2 as the broadening gas in these simulations. While this substitution in the 3D model introduces some uncertainty, still, we can gain a useful estimate of the climate consequences of adding significant amounts of a radiatively inactive broadening gas. We discuss the climate feedback in Section 4.2.

3. Results

3.1. The O_2–CO Runaway

The steady-state abundance of O_2 jumps by seven to eight orders of magnitude to 0.2–2 bar on TRAPPIST-1 e when the CO_2 abundance increases from 0.01 to 0.1 bar (Figure 2, thick lines). The abundance of CO also increases by four to five orders of magnitude to >0.05 bar. The spread of the resultant abundances of O_2 and CO is caused by the uncertainties in their deposition velocities. As we start the calculation from 1 bar N_2 and 0.1 to ~1 bar CO_2, the steady-state atmosphere has O_2 and CO as main components, as well as a substantial abundance of O_3. We thus call this phenomenon "the O_2–CO runaway." The abundance of O_2 continues to gradually increase with more CO_2, but the runaway is partially stabilized by the fact that a higher atmospheric pressure makes the direct recombination reaction between CO and O faster. For TRAPPIST-1 e, the condition for the O_2 runaway coincides with the condition for a global ocean, indicating that a habitable environment on the planet necessarily entails an O_2- and CO-rich atmosphere. For TRAPPIST-1 f and g, more CO_2 is required, and thus the same result applies qualitatively.

Figures 3 and 4 and Table 2 show the vertical profiles of key molecules and the redox fluxes of the scenarios before and after the O_2–CO runaway. The redox balances of the atmosphere and the ocean are well balanced for the models before and after the O_2–CO runaway, and the remaining imbalances are due to a subtle difference between the H_2 mixing ratio on the ground and that at the homopause. The water vapor profile calculated by the 1D photochemistry model agrees well with the mean water vapor profile calculated by the 3D climate model (see Section 4.2). After the O_2–CO runaway, O_2 is essentially well mixed in the atmosphere, and the mixing ratio of O_3 peaks at ~1 mbar (Figure 3). After the O_2–CO runaway, most of the HO_x (OH and HO_2) species combine to form the "reservoir" molecule H_2O_2, and the abundance of the free radical OH is extremely low (Figure 4). This explains the inability of the OH–HO_2 catalytic cycle to recombine CO and O_2. Figure 4 also shows that after the O_2–CO runaway, most of the reactive nitrogen species combine to form HO_2NO_2 above the pressure level of 0.1 bar, the reservoir species for nitrogen. We will discuss the behaviors of nitrogen photochemistry in Section 3.2.

One might ask whether the O_2–CO runaway depends on the assumptions of the boundary conditions, particularly the lack of rapid surface sinks for O_2 and CO. We have explored the impacts of geochemical sinks of O_2 and CO on their atmospheric abundances, and the O_2–CO runaway. The geochemical sinks are expressed in the photochemistry model as the values for the deposition velocity. Conceptually, the transfer flux from the atmosphere to the surface is $\phi = v_{\rm dep\_max}\left(n_0 - \frac{M_0}{\alpha C}\right) = v_{\rm dep} n_0$, where $v_{\rm dep\_max}$ and $v_{\rm dep}$ are the maximum and effective deposition velocities of the gas, n_0 is the gas's number density at the surface, M_0 is the molality in the surface ocean, α is the Henry's law coefficient, and C is a unit conversion constant. The effective deposition velocity thus depends on how quickly the ocean can process the deposited molecule and drive M_0 away from the equilibrium value.

A major potential sink for O_2 is the Fe^{2+} input to the ocean from crustal formation. The O_2 can oxidize Fe^{2+} in the ocean and cause banded iron formation (BIF; $6\,FeO + O_2 \rightarrow 2\,Fe_3O_4$). On Earth, the estimated rate of iron output during the Hamersley BIFs in the late Archean is $\sim 3 \times 10^{12}$ mol yr^{-1}, or 1.1×10^{10} cm^{-2} s^{-1} (Holland 2006). Assuming this entire output of iron is oxidized to Fe_3O_4 in the ocean by O_2, it has two effects: (1) this would correspond to an additional 8×10^9 cm^{-2} s^{-1} equivalent H influx to the atmosphere, doubling the H_2 mixing ratio according to the redox balance; (2) this would be a sink of $\phi_{\rm max} = 2 \times 10^9$ cm^{-2} s^{-1} for O_2. How should this limiting sink be implemented in the photochemistry model? For O_2 under typical conditions, the maximum deposition velocity $v_{\rm dep\_max} = 1.4 \times 10^{-4}$ cm s^{-1}. This $v_{\rm dep\_max}$ is determined by the two-film model of mass transfer between the atmosphere and the ocean (Broecker & Peng 1982) and is related to the piston velocity and is sensitive to the solubility of the gas, the wind speed, and the temperature (Domagal-Goldman et al. 2014; Harman et al. 2015). Therefore, when the surface number density n_0 is small, the rate of deposition is smaller than the limiting sink due to BIF, and $v_{\rm dep}$ should be close to $v_{\rm dep\_max}$. When n_0 is large, the deposition flux is limited by $\phi_{\rm max}$. We therefore implement the lower boundary condition for O_2 due to BIF as follows: if $v_{\rm dep\_max} n_0 < \phi_{\rm max}$, iron oxidation effectively removes O_2 in the ocean, and then $v_{\rm dep} = v_{\rm dep\_max}$; if $v_{\rm dep\_max} n_0 > \phi_{\rm max}$, the deposition velocity is limited by the rate of BIF, or $v_{\rm dep} = \phi_{\rm max}/n_0$.

After implementing this boundary condition and performing another set of simulations, we find that the former condition is met before the O_2–CO runaway, and the latter condition is met after the O_2–CO runaway. In the cases after the O_2–CO runaway, the inclusion of BIF leads to a decrease of the O_2 column abundance by <10%. We therefore conclude that BIF does not substantially impact the onset of the O_2–CO runaway. We note that the rate of iron production during the early Archean (and presumably on a terrestrial exoplanet) may be 20-fold higher than the Hamersley BIFs (Kasting 2013). Here we consider its impact. The 0.1 bar CO_2 case (i.e., the onset of the O_2–CO runaway) has an O_2 number density of 5.5×10^{19} cm^{-3} at the bottom, the full deposition of which would have a flux of 7.7×10^{16} cm^{-2} s^{-1}, about 4×10^7 larger than the flux in the Holland (2006) estimate. Therefore, a 20-fold increase, even if it occurs, would not materially change our results.

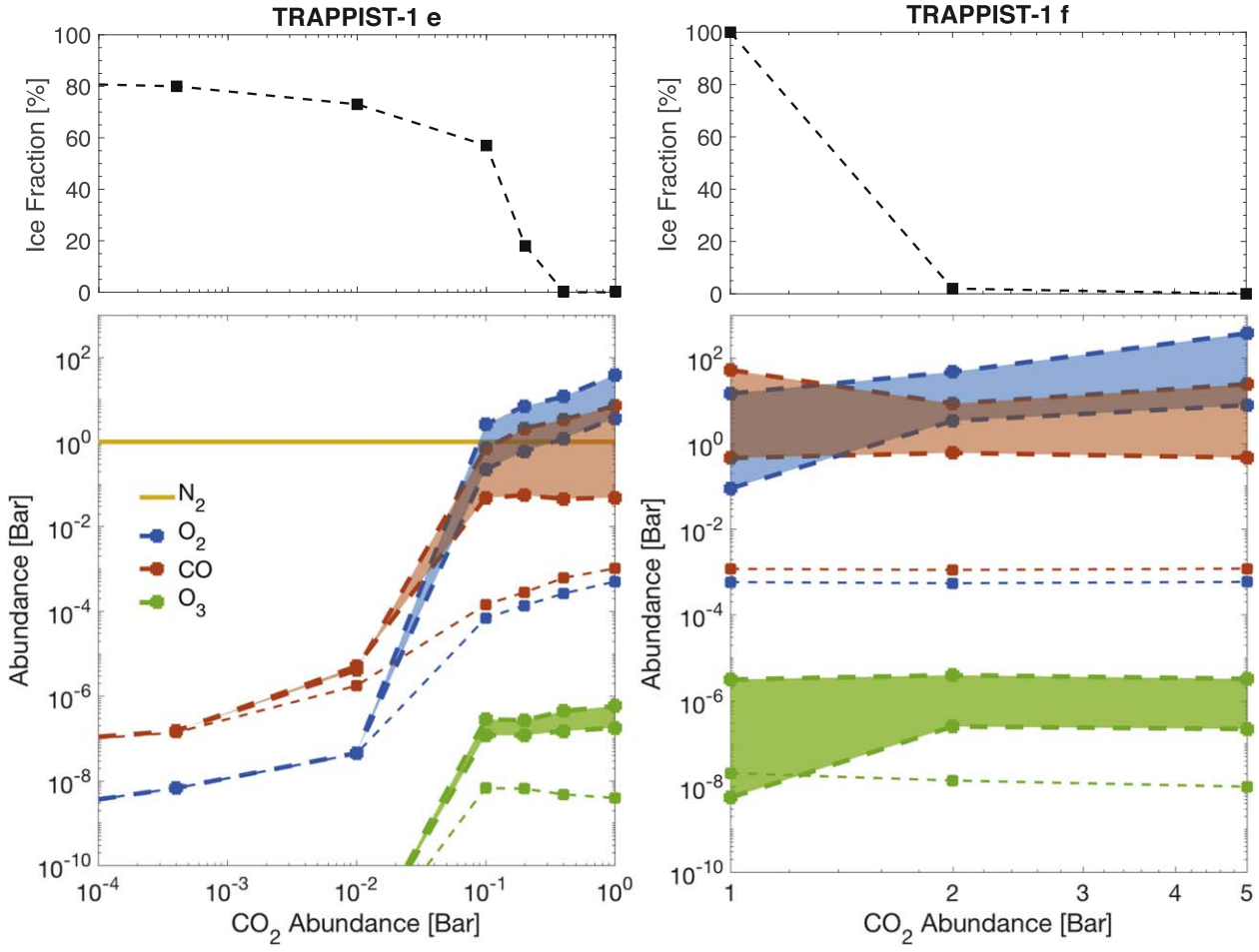

Figure 2. Modeled ice fraction and column-integrated abundances of O_2, CO, and O_3 vs. the abundance of CO_2. Thick lines are the standard models that include known surface sinks of O_2 and CO, and the shaded areas between the thick lines denote the spread of the results, due to the deposition velocity of CO ranging from zero to 10^{-8} cm s^{-1}. The nonzero deposition velocity of CO leads to a higher abundance of O_2 and lower abundance of CO than the zero deposition velocity. Thin lines are the models that additionally assume a direct recombination reaction of O_2 and CO in the ocean. O_2 and CO become main components of the atmosphere when pCO_2 is $\geqslant$0.1 bar; for TRAPPIST-1 e, this jump is roughly coincident with the requirement of a global liquid water ocean.

Additionally, we consider a limiting scenario with direct recombination of O_2 and CO occurring rapidly in the surface ocean. In this case, the effective deposition velocities of O_2 and CO approach their v_{dep_max}, which are mainly controlled by solubilities in the ocean (1.2×10^{-4} cm s^{-1} for CO and 1.4×10^{-4} cm s^{-1} for O_2; Domagal-Goldman et al. 2014). The O_2–CO runaway is prevented in this case, and their abundances max out at 10^{-3}–10^{-4} bar (Figure 1, thin lines). This reaction is performed by aerobic CO-oxidizing bacteria on Earth (King & Weber 2007) and is thus conceivable on an exoplanet with liquid water and abundant O_2 and CO on the surface.

In addition to the sink of O_2, the photochemistry model takes other input parameters such as the NO production rate from lightning, the stellar spectrum, and the deposition velocity of O_3. One might ask whether these parameters significantly bear upon the O_2–CO runaway. We have tested the sensitivity of the model on these parameters using TRAPPSIT-1 e as the test case (Figure 5). First, we find that including a terrestrial rate of NO production by lightning reduces the resulting O_2 partial pressure by only a factor of $\sim$2 in some cases, and the exact value of the lightning production rate near the terrestrial rate has little impact (Figure 5, panel a). This lack of sensitivity has to do the nitrogen photochemistry, which will be discussed in Section 3.2. Second, we find that the onset of the O_2–CO runaway is mildly sensitive to the stellar spectral shape. There is little difference between the standard model and the model using the GJ 876 spectrum. When using the AD Leo spectrum, however, the O_2–CO runaway requires a higher partial pressure of CO_2, $\sim$0.2 bar (Figure 5, panel b). This sensitivity reaffirms the point that the O_2–CO runaway is driven by the high FUV/NUV ratio of the irradiation of late M dwarfs. The AD Leo spectrum has a lower FUV/NUV ratio compared to the GJ 876 spectrum or the assumed TRAPPIST-1 spectrum, and therefore it is less able to drive the O_2–CO runaway. Third, changing the O_3 deposition velocity from the standard value (10^{-3} cm s^{-1}) to a higher value (10^{-1} cm s^{-1}) only has some impact on the case of 0.1 bar CO_2, and overall, it does not affect the onset of the O_2–CO runaway. In sum, the O_2–CO runaway appears to be robust against reasonable uncertainties in the lightning rate, stellar spectrum, and deposition velocities.

3.2. Nitrogen Photochemistry on M Dwarfs' Planets

Our photochemistry models show that nitrogen chemistry in the atmosphere initiated by lightning cannot prevent the O_2–CO runaway. Lightning mainly produces NO in an N_2–CO_2–O_2 atmosphere (Rimmer & Helling 2016; Wong et al. 2017; Harman et al. 2018). Reactive nitrogen species facilitate cycles of OH and HO_2 in Earth's stratosphere and

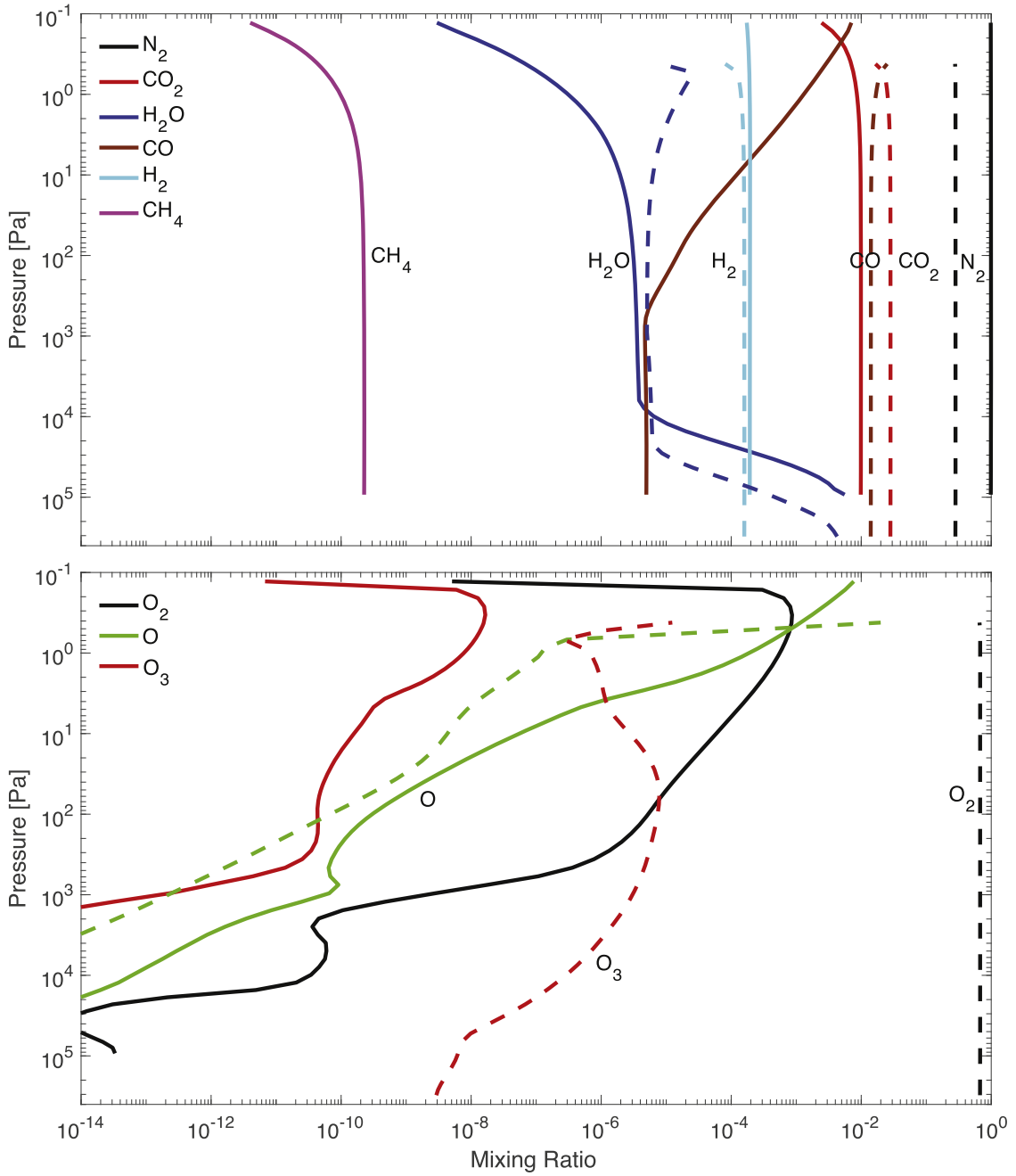

Figure 3. Mixing ratio profiles of background gases and oxygen species without the O_2 runaway (solid lines, 1 bar N_2 with 0.01 bar CO_2) and with the O_2–CO runaway (dashed lines, 1 bar N_2 with 0.1 bar CO_2). The deposition velocity is zero for O_2 and 10^{-8} cm s^{-1} for CO. After the O_2–CO runaway, O2 becomes the dominant gas of the atmosphere, and a substantial O_3 layer forms.

have been suggested to reduce the abundance of accumulated O_2 in CO_2-rich planetary atmospheres by many orders of magnitude (Harman et al. 2018). A main catalytic cycle enabled by reactive nitrogen species is

$$NO + HO_2 \rightarrow NO_2 + OH,$$
$$NO_2 + h\nu \rightarrow NO + O,$$

which is followed by

$$CO + OH \rightarrow CO_2 + H.$$

Our model indicates that the effect of lightning, however, is limited to within a factor of ∼2. This is because most of the reactive species is locked in the reservoir molecules HO_2NO_2 and N_2O_5 (Figure 4), and thus cannot participate in the catalytic cycles. These reservoir molecules are photodissociated by NUV irradiation in Earth's stratosphere, but this photodissociation is severely limited on an M dwarf's planet. HO_2NO_2 also dissociates thermally in the troposphere, but the dissociation in the stratosphere appears to be more important for enabling the catalytic cycles. Our model includes photodissociation of HO_2NO_2 via overtune and combination bands in the near-infrared (Roehl et al. 2002) where an M dwarf's emission is strong, but finds that the total photodissociation rate at the top of the atmosphere is still more than an order of magnitude less

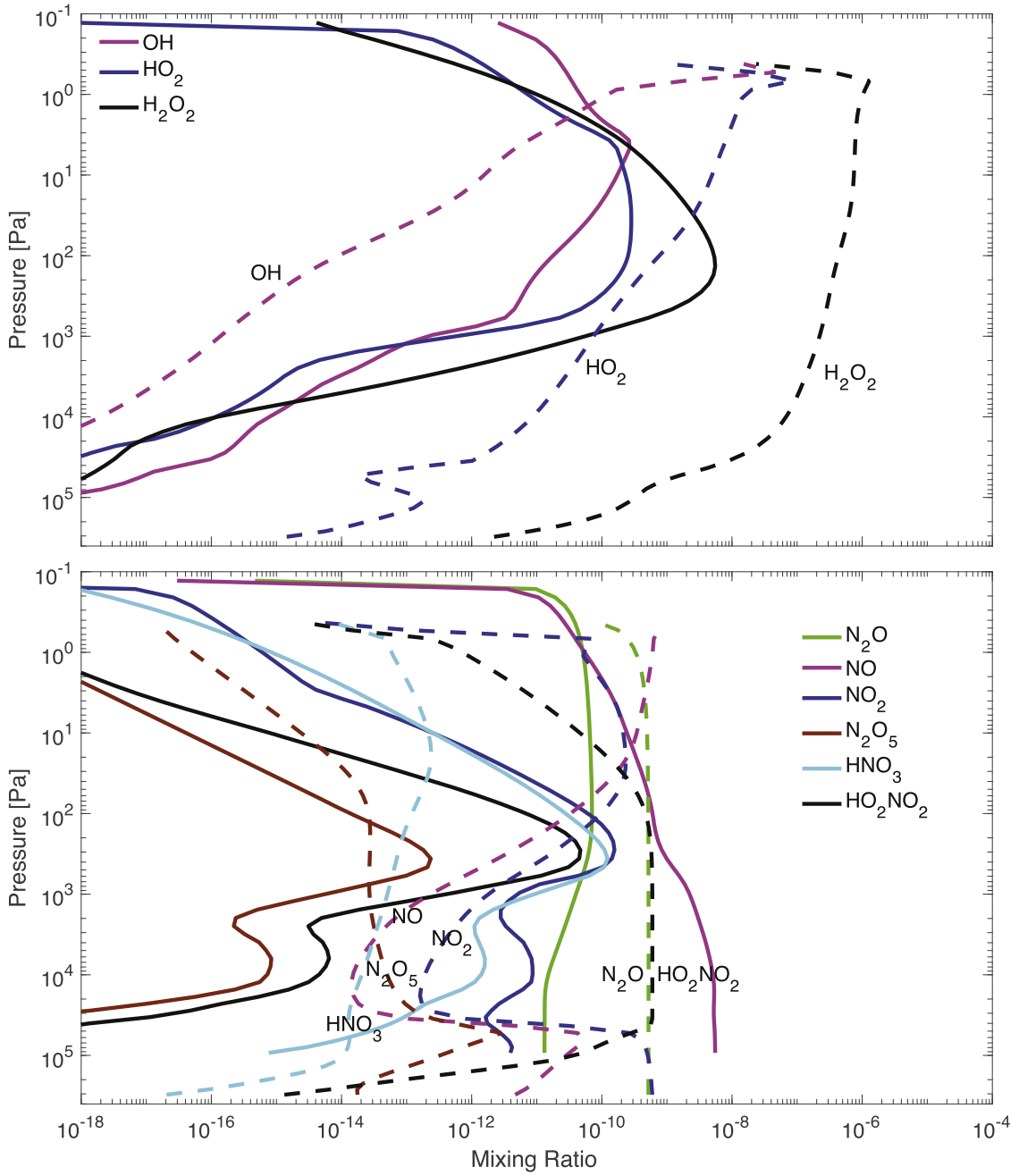

Figure 4. Mixing ratio profiles of reactive hydrogen and nitrogen species without the O_2 runaway (solid lines, 1 bar N_2 with 0.01 bar CO_2) and with the O_2–CO runaway (dashed lines, 1 bar N_2 with 0.1 bar CO_2). The deposition velocity is zero for O_2 and 10^{-8} cm s^{-1} for CO.

than that around a Sun-like star. Additionally, the reservoir molecules are efficiently rained out from the atmosphere. If we do not include HO_2NO_2 or N_2O_5 in the model, we would reproduce the orders-of-magnitude effect by lightning. The detail of nitrogen photochemistry is described in the following.

Harman et al. (2018) found that the steady-state abundance of O_2 would be reduced by many orders of magnitude by including lightning production of NO. Harman et al. (2018), however, did not have HO_2NO_2 or N_2O_5 in their chemical network. Here we perform a set of models with 1 bar N_2 and 0.05 bar CO_2, the same as Harman et al. (2018), with one model using our chemical network and the other without HO_2NO_2 or N_2O_5. The results are compared in Figure 6. To be comparable, the models here are for a hypothetical 1-Earth-radius and 1-Earth-mass planet in the habitable zone of GJ 876. The boundary conditions are the same as the standard models previously described. Because the results are insensitive to the spectral shape changing from the assumed TRAPPIST-1 to GJ 876, the models presented in Figure 6 can also be interpreted in the context of the TRAPPIST-1 models (Figures 2–5) as a case in the middle of the O_2–CO runaway.

If N_2O_5 and HO_2NO_2 (sometimes called HNO_4) are not included in the chemical network, the mixing ratio of O_2 would indeed be reduced by many orders of magnitude (Figure 6,

Table 2
Redox Fluxes of Representative Atmospheric Models for TRAPPIST-1 e[a]

Model	$v_{dep}(CO) = 1E{-}8$ cm s^{-1}	$v_{dep}(O_2) = 0$	$v_{dep}(CO) = 1.2E{-}4$ cm s^{-1}	$v_{dep}(O_2) = 1.4E{-}4$ cm s^{-1}	$v_{dep}(CO) = 0$	$v_{dep}(O_2) = 0$
CO_2	0.01 bar	0.1 bar	0.01 bar	0.1 bar	0.01 bar	0.1 bar
			Escape			
H	−3.1E+8	−2.9E+9	−3.1E+8	−7.1E+8	−3.1E+8	−1.5E+9
H_2	−5.4E+9	−2.8E+9	−5.4E+9	−5.0E+9	−5.4E+9	−4.2E+9
Total	−5.7E+9	−5.7E+9	−5.7E+9	−5.7E+9	−5.7E+9	−5.7E+9
			Outgassing			
H_2	3.0E+9	3.0E+9	3.0E+9	3.0E+9	3.0E+9	3.0E+9
CO	3.0E+9	3.0E+9	3.0E+9	3.0E+9	3.0E+9	3.0E+9
H_2S	9.0E+8	9.0E+8	9.0E+8	9.0E+8	9.0E+8	9.0E+8
NO[b]	−1.2E+9	−1.2E+9	−1.2E+9	−1.2E+9	−1.2E+9	−1.2E+9
Total	5.7E+9	5.7E+9	5.7E+9	5.7E+9	5.7E+9	5.7E+9
			Dry and Wet Deposition			
O_2	⋯	⋯	⋯	7.9E+11	⋯	⋯
O_3	⋯	3.4E+9	⋯	2.7E+8	⋯	3.4E+8
HO_2	⋯	2.9E+5	⋯	1.5E+8	⋯	1.4E+7
H_2O_2	⋯	5.8E+7	⋯	1.1E+10	⋯	4.7E+9
CO	−2.0E+6	−1.1E+10	−9.1E+9	−8.1E+11	⋯	⋯
CH_2O	−2.8E+6	⋯	−7.8E+5	⋯	−2.8E+6	⋯
CHO_2	−2.4E+6	⋯	⋯	⋯	−2.4E+6	⋯
H_2S	−1.1E+8	−9.0E+8	−1.1E+8	−3.7E+8	−1.1E+8	−8.5E+8
H_2SO_4	1.0E+7	⋯	1.7E+7	9.9E+6	1.0E+7	⋯
NO	1.1E+8	⋯	1.6E+8	⋯	1.1E+8	⋯
NO_2	1.7E+6	4.0E+8	2.7E+6	1.9E+7	1.7E+6	1.8E+8
NO_3	⋯	1.3E+9	⋯	5.4E+6	⋯	2.4E+7
N_2O_5	⋯	1.2E+9	⋯	2.4E+5	⋯	1.3E+7
HNO	5.1E+8	⋯	4.5E+8	⋯	5.1E+8	⋯
HNO_2	2.6E+7	1.3E+8	5.8E+7	1.8E+9	2.6E+7	1.6E+9
HNO_3	3.6E+6	1.1E+5	9.7E+6	1.4E+7	3.6E+6	5.0E+4
HNO_4	⋯	2.2E+6	⋯	1.7E+7	⋯	3.0E+7
Total	5.4E+8	−5.0E+9	−8.5E+9	−4.1E+9	5.5E+8	6.0E+9
			Return H_2 Flux			
H_2	−5.5E+8	5.0E+09	8.5E+9	4.1E+9	−5.5E+8	−6.1E+9
			Overall Flux Balance			
	1.0E+4	1.1E+6	1.1E+7	−7.9E+6	8.6E+5	−4.5E+6

Notes.
[a] The redox flux is expressed as the equivalent of unit H influx to the atmosphere and has a unit of cm^{-2} s^{-1}. H_2O, CO_2, N_2, and SO_2 are defined as redox neutral. For example, deposition of a CO molecule would create a redox flux of −2, and deposition of a O_3 molecule would create a redox flux of +6.
[b] The NO flux is included to simulate lightning production of NO.

dashed lines). The O_3 would be almost completely removed. This result is consistent with Harman et al. (2018) in terms of the effect of the NO and NO_2 cycle and in general with the basic understanding of terrestrial atmospheric chemistry, that the NO and NO_2 cycle help reduce O_3. Note that the amount of O_2 near the surface is still much higher than that in Harman et al. (2018), which may be due to different choices of species in photochemical equilibrium and different boundary conditions assumed (Section 4.1). When N_2O_5 and HO_2NO_2 are included in the chemical network, the results are dramatically different. We see that (1) most of the nitrogen other than N_2 or N_2O are locked in the form of HO_2NO_2 in the stratosphere, and the N_2O_5 reservoir is also significant (Figure 6, solid lines, also in Figure 4, dashed lines); (2) summing the reactive nitrogen species (nitrogen species other than N_2 or N_2O), the mixing ratio is smaller than the case without N_2O_5 or HO_2NO_2; and (3) the mixing ratio of O_2 remains constant throughout the atmosphere rather than being reduced by many orders of magnitude.

Why does including N_2O_5 and HO_2NO_2 in the chemical network have such a large effect? In the stratosphere, HO_2NO_2 is formed by the following combination reaction:

$$HO_2 + NO_2 + M \rightarrow HO_2NO_2 + M$$

and destroyed by photolysis

$$HO_2NO_2 + h\nu \rightarrow HO_2 + NO_2$$

$$HO_2NO_2 + h\nu \rightarrow HO + NO_3$$

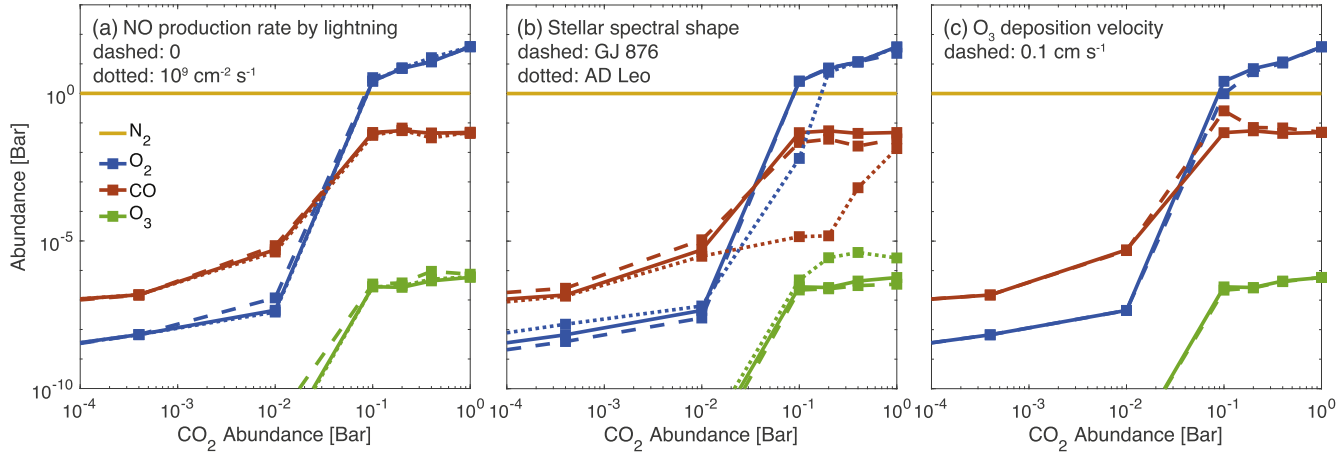

Figure 5. Sensitivity of the onset of the O_2–CO runaway to the lightning rate, the stellar spectral shape, and the deposition velocity of O_3. The sensitivity studies are performed on the models of TRAPPSIT-1 e, and the results from varied parameters are shown with the respective line styles. The solid lines are from the standard model. The onset of the O_2–CO runaway is not sensitive to the lightning rate or the deposition velocity of O_3, and it is mildly sensitive to the spectral shape.

and reaction with OH

$$HO_2NO_2 + OH \rightarrow H_2O + NO_2 + O_2.$$

Similarly, for N_2O_5, its formation is by combination of NO_2 and NO_3, and its depletion is by photolysis.

HO_2NO_2 and N_2O_5 are important species in Earth's atmosphere but they do not overtake NO or NO_2 as the main reactive nitrogen species. Under the conditions that correspond to present-day Earth's midlatitude, our model predicted mixing ratio profiles of NO, NO_2, N_2O_5, HNO_3, and HO_2NO_2 in the middle atmosphere that are fully consistent with measurements from balloons (Sen et al. 1998; Hu 2013). On a terrestrial planet of M-dwarf stars, however, the UV irradiation flux that drives the photolysis of HO_2NO_2 and N_2O_5 is more than one order of magnitude lower (Table 3), and therefore, these species can accumulate to a higher abundance, overtaking NO or NO_2 as the main reactive nitrogen reservoir. This is what we see in the solid lines of Figure 6. We have included the photodissociation of HO_2NO_2 via overtone and combination bands in the near-infrared (Roehl et al. 2002) in our calculations, because the near-infrared irradiation on a planet in the habitable zone of M-dwarf stars is comparable to that of Sun-like stars. Table 3 indicates that while the near-infrared dissociation contributes dominantly to the total dissociation rate, the total dissociation rate is still more than one order of magnitude less than the value for Sun-like stars.

Additionally, more nitrogen in HO_2NO_2 and N_2O_5 leads to more rapid removal of reactive nitrogen from the atmosphere. Without these species, the only effective removal pathway of reactive nitrogen is the deposition and rain out of HNO, HNO_2, and HNO_3. It is well known that HO_2NO_2 and N_2O_5 are highly soluble or reactive in water and rain out very efficiently. Also, heterogeneous reactions of N_2O_5 on and within atmospheric aerosols or cloud droplets further facilitate rain out (Wang et al. 2017). Therefore, the formation of these species leads to more rapid removal and reduction of the total reactive nitrogen mixing ratio, as we see in Figure 6.

Finally, we point out that the atmosphere has a substantial amount (1 ppb) of N_2O produced abiotically. The production path is

$$N_2 + O(^1D) + M \rightarrow N_2O + M.$$

The kinetic rate of this reaction was measured recently (Estupinán et al. 2002), and this reaction is not typically included in photochemistry models of planetary atmospheres. Again because of the low NUV irradiation, this abiotic N_2O can accumulate to 1 ppb in the atmospheres of TRAPPIST-1 planets. The longer lifetime of N_2O in planetary atmospheres around M stars has been suggested previously (Segura et al. 2005). Notably, this N_2O is the source of NO and NO_2 in the upper atmosphere (Figure 6), via

$$N_2O + O(^1D) \rightarrow NO + NO.$$

This source of NO exists without any lightning events. It is therefore necessary to also include N_2O in the photochemical model of rocky and potentially habitable planets around M-dwarf stars.

4. Discussion

4.1. Comparison with Prior Studies

To further confirm that the O_2 and CO buildup we found is not a model artifact, we compare with two prior studies that studied N_2–CO_2 atmospheres of terrestrial planets in the habitable zone of M-dwarf stars (Tian et al. 2014; Harman et al. 2015). The two studies built models for a hypothetical 1-Earth-radius and 1-Earth-mass planet, having 1 bar N_2 atmosphere with 0.05 bar CO_2. Note that the level of CO_2 they assumed is less than the level of CO_2 required for global habitability on TRAPPIST-1 e. Both studies used the habitable zone of GJ 876 as the representative case, and applied the same method to maintain the redox balance of both the atmosphere and the ocean (i.e., the pseudo H_2 flux). For comparison, we set up a model of a 1-Earth-radius and 1-Earth-mass planet, having 1 bar N_2 atmosphere with 0.05 bar CO_2, at the 0.21 au orbital distance from the M star GJ 876. We set up the same pressure–temperature profile as Tian et al. (2014), i.e., the surface temperature of 288 K and the stratosphere temperature of 180 K. We use the same profile of the eddy diffusion coefficient from terrestrial measurements, adopted by Tian et al. (2014). While these factors are not explicitly stated, we suspect that they are treated the same way as in Harman et al. (2015). We use the same emission rates as these works: the emission rate of H_2 is $10^{10}\,cm^{-2}\,s^{-1}$, and that of other gases is zero. Note that our models have a more expanded chemical network including HO_2NO_2 and N_2O_5, and the choices of species in photochemical

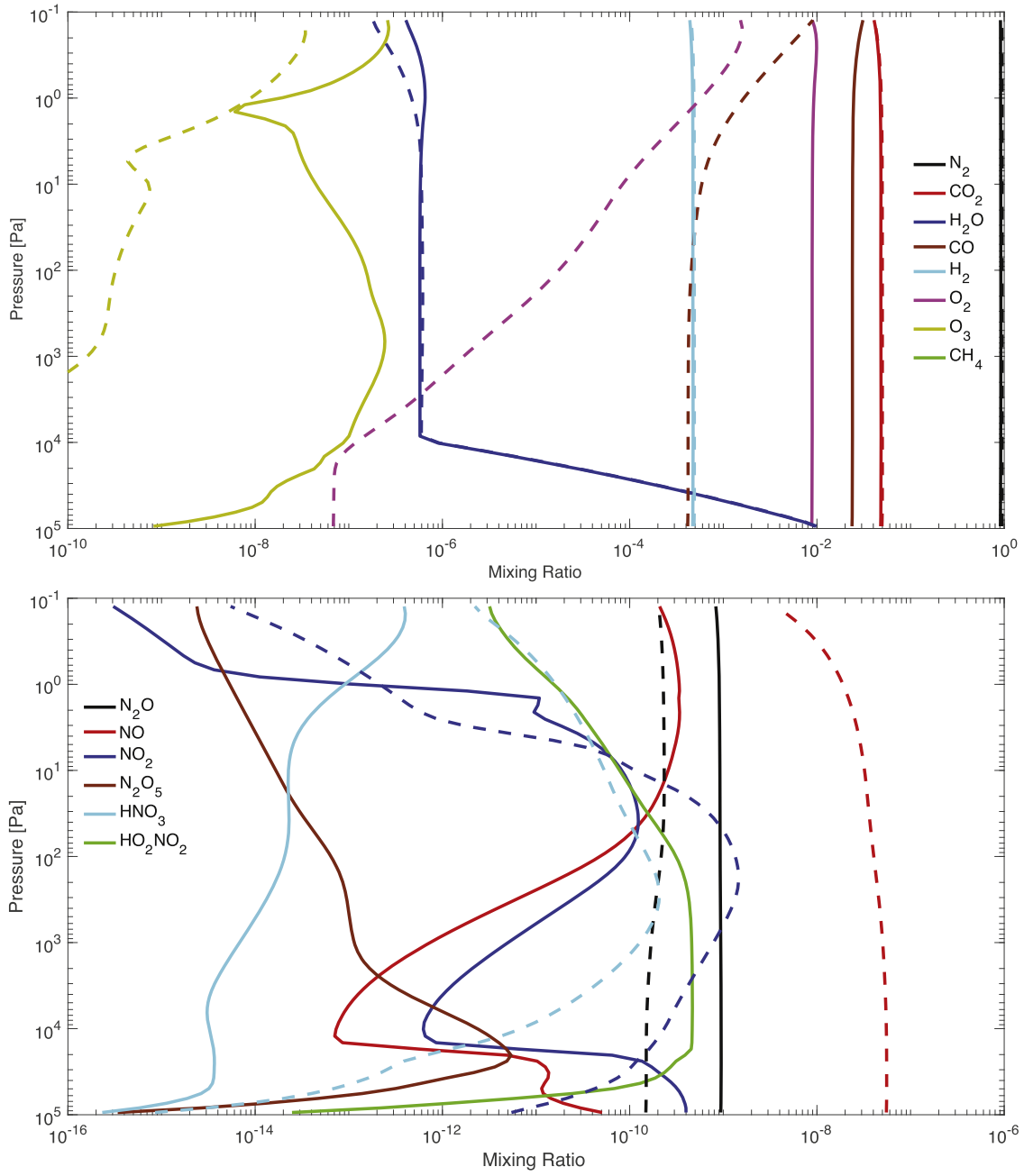

Figure 6. Atmospheric models with 1 bar N_2 and 0.05 bar CO_2, including a NO source of 6×10^8 molecule cm^{-2} s^{-1} at the surface mimicking the effect of lightning (solid lines), and the same NO source but without N_2O_5 or HO_2NO_2 in the chemical network (dashed lines). These models use the stellar spectrum of GJ 876, corresponding to Harman et al. 2018). The effect of lightning is limited when the reservoir molecules are included in the chemical network.

Table 3
Top-of-atmosphere Photolysis Rates (J values) of HO_2NO_2 and N_2O_5 on Earth and on TRAPPIST-1 e

Reaction	J Earth (s^{-1})	J TRAPPIST-1 e (s^{-1})	Of Which Caused by Near-infrared Irradiation
$HO_2NO_2 + h\nu \rightarrow HO_2 + NO_2$	1.83×10^{-4}	9.66×10^{-6}	6.28×10^{-6}
$HO_2NO_2 + h\nu \rightarrow HO + NO_3$	4.89×10^{-5}	8.90×10^{-7}	0
$N_2O_5 + h\nu \rightarrow NO_3 + NO_2$	4.82×10^{-5}	6.56×10^{-7}	0
$N_2O_5 + h\nu \rightarrow NO_3 + NO + O$	1.45×10^{-4}	2.52×10^{-6}	0

Note. The contribution from the overtone and combination bands of HO_2NO_2 in the near-infrared to the J values for TRAPPIST-1 e is also shown.

equilibrium are typically different between photochemical models.

The main difference between Tian et al. (2014) and Harman et al. (2015) is in the deposition velocities. We adopt the deposition velocities that each work used. In Tian et al. (2014), the deposition velocities of CO and O_2 are 10^{-6} cm s^{-1}, and O_3 as a long-lived species has a deposition velocity of 10^{-3} cm s^{-1}. Figure 7 shows our results in this case. The

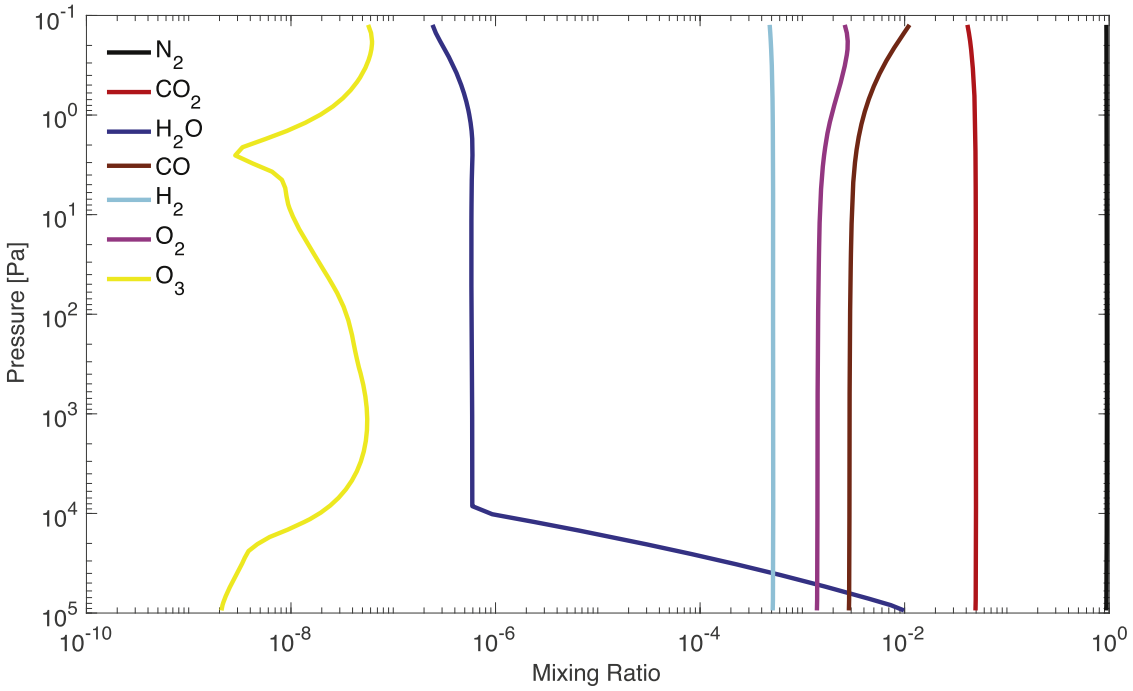

Figure 7. Results using the same parameters as Tian et al. (2014).

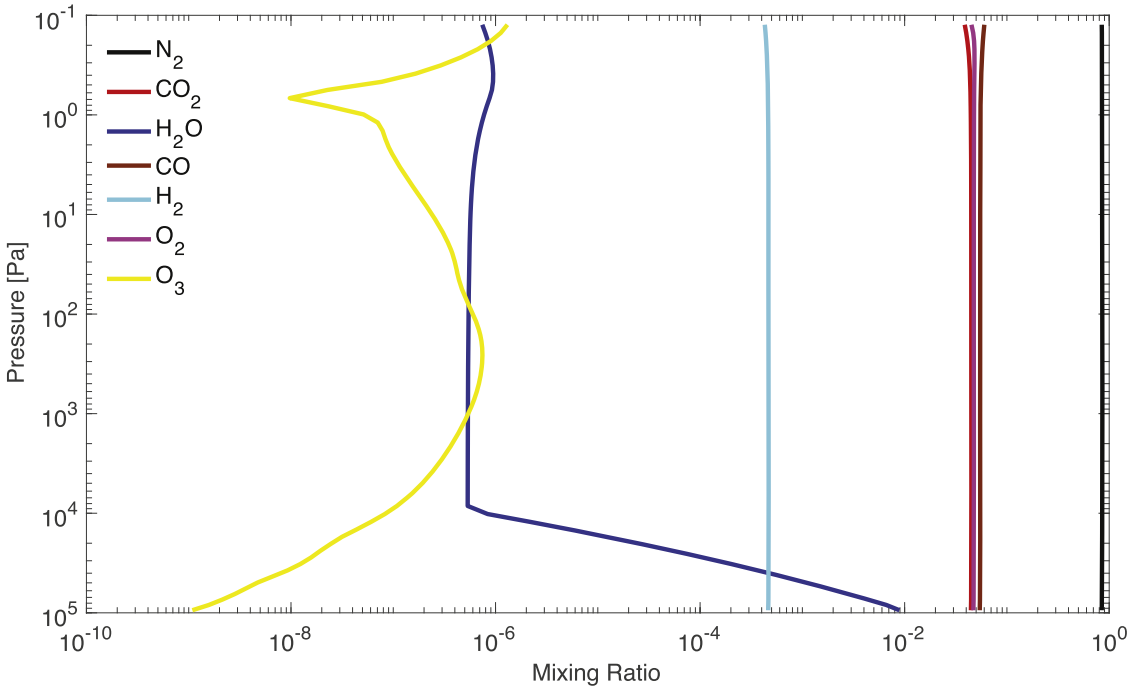

Figure 8. Results using the same parameters as Harman et al. (2015).

results are sufficiently consistent with Tian et al. (2014) in terms of the mixing ratios of CO and O_2, as well as the peak mixing ratio of O_3.

Harman et al. (2015) assumed a deposition velocity of 10^{-8} cm s^{-1} for CO, and zero for O_2, and assumed O_3 to be a short-lived species. The amount of O_2 in our result is consistent with Harman et al. (2015); however, the amount of CO in our result is a factor of a few greater (Figure 8). The difference may be due to the fact that the model of Harman et al. (2015) had 15 species assumed to be in photochemical equilibrium, while our model does not have any.

Note that the O_2 column abundance in both cases, assuming 0.05 bar CO_2, falls between the value for 0.01 bar CO_2 and 0.1 bar CO_2 in our TRAPPIST-1 e models (Figure 2). This comparison shows that the 0.05 bar CO_2 case that the previous studies have assumed happens to be in the transition into the O_2–CO runaway. A small increase in the CO_2 partial pressure will lead to a large increase in the accumulation of photochemical O_2. Comparing Figures 7 and 8, we find that assuming O_3 to be one of the species in photochemical equilibrium, or not, introduces substantial variation to the model results. O_3 may have substantial abundance at the

Table 4
New Climate Scenarios Modeled for This Study and Their Key Climate Characteristics

Planet	N_2	CO_2	*T* Surf Globe (K)	Ice Fraction
TRAPPIST-1 e	1 bar	0.1 bar	274	57%
TRAPPIST-1 e	1.5 bar	0.1 bar	286	12%
TRAPPIST-1 e	2 bar	0.1 bar	291	0.3%
TRAPPIST-1 e	4 bar	0.1 bar	320	0%
TRAPPIST-1 e	1 bar	0.2 bar	285	18%
TRAPPIST-1 e	1.5 bar	0.2 bar	297	0%
TRAPPIST-1 e	2 bar	0.2 bar	308	0%
TRAPPIST-1 e	4 bar	0.2 bar	332	0%

surface, and its deposition may contribute to the overall redox balance of the atmosphere (Table 2).

4.2. Climate Feedback of the O_2–CO Runaway

As photochemically produced O_2 and CO become main constituents in the atmosphere, they contribute meaningfully to the total pressure. O_2 has no strong infrared absorption bands, and CO absorption occurs only at the shoulders of the planetary thermal emission spectra. Their primary contribution to radiation is through the pressure broadening of CO_2 absorption lines and Rayleigh scattering, with the pressure broadening effect being the dominant of the two (Goldblatt et al. 2009). Several additional 3D climate model simulations are conducted newly for this work to test the effects of increased broadening gas partial pressures on the climate of TRAPPIST-1 e, summarized in Table 4. Three-dimensional simulations are conducted for TRAPPIST-1 e with 0.1 bar and 0.2 bar CO_2, and with broadening gas partial pressures of 1.5, 2, and 4 bar, respectively.

The results of the 3D climate models with increased atmospheric pressure are shown in Figure 9. Using a 3D climate model, we can self-consistently incorporate the effects of pressure broadening and Rayleigh scattering, along with resultant climatological feedbacks. Increasing the background pressure by up to 4 folds yields increases to the global mean surface temperature by a few tens of Kelvin; even though significant, this does not change the general assessment regarding habitability for atmospheres with $\leqslant$0.2 bar CO_2. However, for higher background pressures produced by larger CO_2 amounts, the combined effects may cause TRAPPIST-1 e to become too hot to be reasonably habitable. In addition, O_3 is a greenhouse gas with an absorption band in the middle of the planetary thermal emission spectra (9.6 μm). At expected concentrations, however, its contribution to the greenhouse effect is dwarfed by that of CO_2 and H_2O (Kiehl & Trenberth 1997), and thus would not significantly raise the surface temperature. Given the O_2 runaway and the climate models, we conclude that for TRAPPIST-1 e to remain globally habitable, it must have pCO_2 in a somewhat narrow range between 0.01 and 0.2 bar.

One might wonder if substituting O_2/CO with N_2 in the climate model is reasonable. O_2/CO and N_2 have mean molecular weights within ~15%, specific heats within ~10%, and neither have strong absorption bands in the planetary thermal emission spectra. Both O_2 and N_2 are diatomic molecules and thus do not have vibrational or rotational absorption modes, and thus are not conventional greenhouse gases. The absorption feature of CO at ~100 μm is swamped

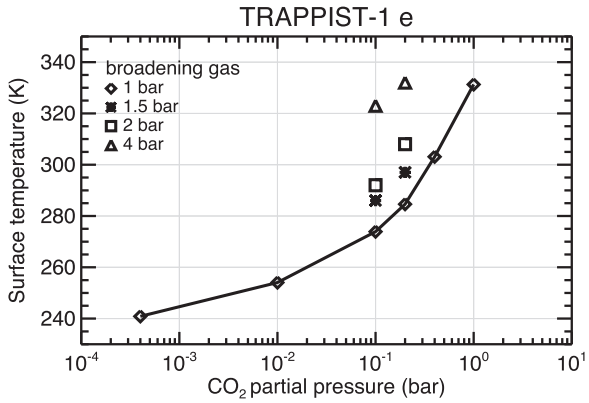

Figure 9. Global mean surface temperature of TRAPPIST-1 e vs. the abundance of CO_2 (*x*-axis) and the broadening gas amount (legend). The temperature is calculated in 3D climate model simulations, with the H_2O abundance and the cloud feedback self-consistently modeled (Wolf 2017). We consider increases to the total pressure by increasing the N_2 background amount, rather than including O_2 or CO explicitly in the climate model. Increasing the background pressure results in meaningful increases in the mean surface temperature.

by H_2O rotational-vibration absorption bands. The feature of CO at ~5 μm may show through both CO_2 and H_2O, but this spectral region is located where both thermal emitted and incident stellar radiation are relatively small. In addition, in sufficiently dense atmospheres each molecular pair features collision-induced absorption (CIA) in the infrared, which can affect climate. But, in moist atmospheres, as modeled here, O_2–O_2 CIA at 6.4 μm is swamped by the H_2O feature in this same spectral region (Hopfner et al. 2012), and N_2–N_2 CIA, which affects wavelengths longward of ~30 μm, is swamped by H_2O rotational-vibration absorption bands (Wordsworth & Pierrehumbert 2013). In total, the radiative effects of O_2, CO, and N_2 are primarily felt indirectly through their contribution to the total atmospheric pressure and in the subsequent pressure broadening of CO_2 absorption features, which can have a significant warming effect on climate (Goldblatt et al. 2009). Collisions between molecules shift absorption from line centers toward the wings, with the end result being more total radiation being absorbed.

Increasing the total pressure of the atmosphere also increases Rayleigh scattering, which would act to cool the planet, counteracting the above discussed effect of pressure broadening. However, the increase in greenhouse forcing from enhanced pressure broadening dominates over the increase in reflection due to enhanced Rayleigh scatterings (Goldblatt et al. 2009). Note that the Rayleigh scattering cross sections for O_2, CO, and N_2 are also quite close (Thalman et al. 2014). CO has an absorption band at ~2.3 μm, and this band contributes to near-infrared absorption of stellar radiation from TRAPPIST-1. However, the near-infrared absorption of CO_2 and H_2O will be more significant. Thus, substituting N_2 for O_2 and CO in our model should not give rise to a large error in thermal or stellar forcings.

Our atmospheric chemistry model also predicts that the O_2-rich atmospheres on TRAPPIST-1 planets should have a significant O_3 layer (Figure 3), and this is consistent with previous models of O_2-rich planets found around M-dwarf stars (Segura et al. 2005; Meadows et al. 2018). That O_3 is also absent from our 3D climate model. However, note that because M-dwarf stars emit several orders of magnitude less radiation in the NUV region ($\lambda \geqslant 200$ nm), a stratospheric O_3 layer would

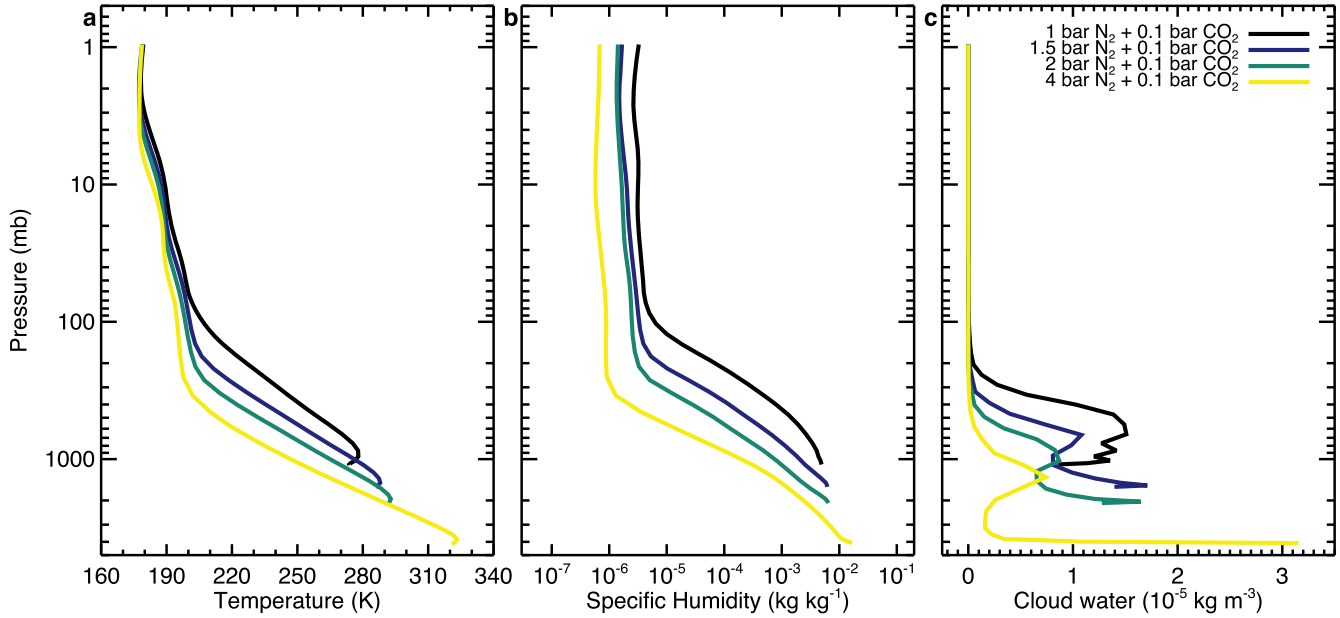

Figure 10. Global mean temperature and water profiles of 3D climate models assuming a varied background N_2 partial pressure for TRAPPIST-1 e. The water vapor profiles are largely consistent with the profiles predicted by our 1D photochemistry model (Figure 3). The stratosphere remains cold and water-depleted when more than 1 bar of N_2 is assumed.

have little radiation to absorb and would not form a stratospheric inversion. Indeed, simulations of O_2-rich planets around M-dwarf stars indicate that the stratospheric temperatures would remain cold (Segura et al. 2005; Meadows et al. 2018). While O_3 is a greenhouse gas, with an absorption band at 9.6 μm, at expected concentrations its contribution to the greenhouse effect is dwarfed by those of CO_2 and H_2O (Kiehl & Trenberth 1997), and thus is not a significant driver of climate change. Based on the above discussions, we feel that substituting N_2 for O_2 and CO will not radically alter the resultant climates in our 3D model, and provides useful estimates for climate change for TRAPPIST-1 e under thicker atmospheres.

Finally, we briefly discuss "the feedback of the feedback:" the effect of the changed temperature profile after the O_2–CO runaway onto the atmospheric photochemistry itself. Figure 10 shows the mean pressure–temperature and water profiles from the 3D climate models assuming varied partial pressure of N_2. The similarity of these profiles is striking: the stratosphere's temperature and water vapor abundance stay low, and only the lowest layers of the atmosphere experience higher temperatures after the O_2–CO runaway. As such, even though new photochemical simulations were not performed with the new climate studies, the change in the temperature profile and its impact on the atmospheric chemistry is likely limited to the bottom layers of the atmosphere, and thus unlikely to significantly affect the O_2–CO runaway.

4.3. Geologic Context for the O_2–CO Runaway

Silicate weathering, if it occurs on a rocky planet, helps keep pCO_2 in a desirable range that is consistent with a liquid water ocean (Walker et al. 1981). The O_2–CO runaway, together with the enhanced warming due to pressure broadening, increases the sensitivity of the surface temperature on pCO_2. This increased sensitivity would allow silicate weathering to maintain pCO_2 in the required narrow range.

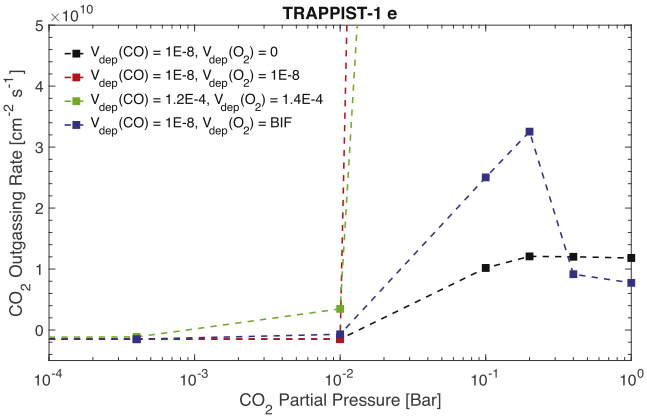

Figure 11. Outgassing rate of CO_2 implied by the CO_2 partial pressure for varied assumptions of the deposition velocities (cm s^{-1}). The outgassing rate by ridge volcanism on Earth is $0.4 \sim 1 \times 10^{10}$ cm^{-2} s^{-1} (Sleep & Zahnle 2001). When the CO_2 partial pressure is small, a small negative value for the outgassing rate is implied; this is because a fixed outgassing rate of CO is assumed.

Another question is whether the O_2–CO runaway state is sustainable. Our photochemistry models assume fixed column abundances of CO_2 and therefore imply appropriate rates of volcanic outgassing that maintain the fixed abundances. Figure 11 shows the implied CO_2 outgassing rate for varied assumptions of the deposition velocities. We see that in the standard models, as well as the models including the BIF as the sink for O_2, the implied CO_2 outgassing rate of the runaway scenarios is close to the outgassing rate by ridge volcanism on present-day Earth (Figure 11, black and blue lines). In those cases, the O_2–CO runaway state is well sustained by a reasonable rate of replenishment from the planetary interior. However, if a fixed deposition velocity for O_2 is used, even as small as 10^{-8} cm s^{-1} presumably due to recombination in hydrothermal flows, a very large CO_2 outgassing rate would be required to sustain the runaway state (i.e., out of limit on Figure 11, red lines). Is this scenario realistic? In fact, the

implied CO_2 outgassing rate does not necessarily come from the interior of the planet as "new" CO_2; instead, the very recombination process in hydrothermal flows that consumes O_2 will produce CO_2. The O_2–CO runaway state would therefore be sustainable via cycling through the deep ocean. Lastly, when the surface-ocean recombination of CO and O_2 is assumed, the O_2–CO runaway does not occur (Figure 2), but a large "outgassing rate" is still required for $pCO_2 > 0.1$ bar. This outgassing rate can be sustained by the product of the recombination itself. In all, the O_2–CO runaway appears to be sustainable from a geochemical point of view, and the sustainability may involve replenishment of CO_2 from the planetary interior, or cycling of CO, O_2, and CO_2 through the deep ocean.

As such, the O_2- and CO-rich atmosphere modeled here does not require any planetary outgassing outside of typical geological regimes; neither does it require a highly oxidized or dried upper mantle, presumably produced by loss of hydrogen into space over a long active period of the M dwarfs (Luger & Barnes 2015; Tian & Ida 2015; Bolmont et al. 2017). The atmosphere modeled here has O_2 and CO coexisting at large abundances, different from the predicted massive O_2 atmospheres from accumulative hydrogen loss that would have little CO (Bolmont et al. 2017; Lincowski et al. 2018).

5. Conclusion

We use an atmospheric photochemistry model to study the effect of stellar UV radiation on the varied abundance of CO_2 on the rocky planets in the habitable zone of the late M dwarf TRAPPIST-1. Our models show that for a small abundance of CO_2, an atmosphere with O_2 and CO as the main components would be the steady state. This "O_2–CO runaway" is robust against the nitrogen catalytical cycles from lightning, reasonable uncertainties in the stellar spectrum, as well as various geochemical sinks for O_2 and CO, including the BIF. For the planets TRAPPIST-1 e, f, and g, because they require sizable abundance of CO_2 to be habitable, the models presented here imply that virtually all habitable scenarios of the TRAPPSIT-1 planets entail an O_2-rich atmosphere. The O_2–CO runaway can only be prevented by assuming a direct recombination of O_2 and CO in the surface ocean, which would probably require biochemistry.

The O_2–CO runaway mechanism described here also applies to temperate and rocky planets of other low-temperature M-dwarf stars, a few tens of which are expected to be discovered by the *TESS* mission (Sullivan et al. 2015). This is because the cause of the runaway, the strong FUV and weak NUV irradiation, applies to many moderately active M-dwarf stars (Loyd et al. 2016). The calculations presented here not only show that the spectral features of O_2 and O_3 cannot be regarded as robust signs of biogenic photosynthesis (Domagal-Goldman et al. 2014; Tian et al. 2014; Harman et al. 2015), but also show that O_2 and CO are likely dominant gases on habitable planets of M-dwarf stars. These gases have spectral features suitable for detection with high-resolution spectroscopy (Snellen et al. 2010; Lovis et al. 2017). The absorption features of O_2, O_3, CO, and CO_2, as well as the CIA features of O_2 (Misra et al. 2014; Lincowski et al. 2018), should therefore be the first choices for observation programs to characterize the atmospheres of temperate and rocky planets of M-dwarf stars.

We thank Y. L. Yung, J. F. Kasting, C. E. Harman, and S. Seager for a helpful discussion of atmospheric photochemistry. R.Y.H. was supported by NASA grant No. 80NM0018F0612 and grant No. 15038.004 from the Space Telescope Science Institute, which is operated by AURA, Inc., under NASA contract NAS 5-26555. The research was carried out at the Jet Propulsion Laboratory, California Institute of Technology, under a contract with the National Aeronautics and Space Administration.

ORCID iDs

Renyu Hu https://orcid.org/0000-0003-2215-8485
Eric T. Wolf https://orcid.org/0000-0002-7188-1648

References

Beichman, C., Benneke, B., Knutson, H., et al. 2014, PASP, 126, 1134
Bolmont, E., Selsis, F., Owen, J. E., et al. 2017, MNRAS, 464, 3728
Bourrier, V., Ehrenreich, D., Wheatley, P. J., et al. 2017, A&A, 599, L3
Broecker, W. S., & Peng, T. H. 1982, Tracers in the Sea (Palisades, NY: Lamont-Doherty Geological Observatory)
De Wit, J., Wakeford, H. R., Lewis, N. K., et al. 2018, NatAs, 2, 214
Dittmann, J. A., Irwin, J. M., Charbonneau, D., et al. 2017, Natur, 544, 333
Domagal-Goldman, S. D., Segura, A., Claire, M. W., Robinson, T. D., & Meadows, V. S. 2014, ApJ, 792, 90
Estupinán, E. G., Nicovich, J. M., Li, J., Cunnold, D. M., & Wine, P. H. 2002, JPCA, 106, 5880
France, K., Froning, C. S., Linsky, J. L., et al. 2013, ApJ, 763, 149
France, K., Loyd, R. P., Youngblood, A., et al. 2016, ApJ, 820, 89
Gaillard, F., & Scaillet, B. 2014, E&PSL, 403, 307
Gao, P., Hu, R., Robinson, T. D., Li, C., & Yung, Y. L. 2015, ApJ, 806, 249
Gillon, M., Triaud, A. H., Demory, B. O., et al. 2017, Natur, 542, 456
Goldblatt, C., Claire, M. W., Lenton, T. M., et al. 2009, NatGe, 2, 891
Grimm, S. L., Demory, B. O., Gillon, M., et al. 2018, A&A, 613, A68
Hardacre, C., Wild, O., & Emberson, L. 2015, ACP, 15, 6419
Harman, C. E., Felton, R., Hu, R., et al. 2018, ApJ, 866, 56
Harman, C. E., Schwieterman, E. W., Schottelkotte, J. C., & Kasting, J. F. 2015, ApJ, 812, 137
Holland, H. D. 2006, RSPTB, 361, 903
Hopfner, M., Milz, M., Buehler, S., Orphal, J., & Still, G. 2012, GeoRL, 39, L10706
Hu, R. 2013, Doctoral dissertation, MIT
Hu, R., Seager, S., & Bains, W. 2012, ApJ, 761, 166
Hu, R., Seager, S., & Bains, W. 2013, ApJ, 769, 6
James, T. S., & Hu, R. 2018, ApJ, 867, 17
Kasting, J. F. 2013, ChGeo, 362, 13
Kharecha, P., Kasting, J., & Siefert, J. 2005, Geobiology, 3, 53
Kiehl, J. T., & Trenberth, K. E. 1997, Earth's Annual Global Mean Energy Budget. Bull. Amer. Meteo. Soc, 78, 197
King, G. M., & Weber, C. F. 2007, Nature Reviews Microbiology, 5, 107
Lincowski, A. P., Meadows, V. S., Crisp, D., et al. 2018, ApJ, 867, 76
Lovis, C., Snellen, I., Mouillet, D., et al. 2017, A&A, 599, A16
Loyd, R. P., France, K., Youngblood, A., et al. 2016, ApJ, 824, 102
Luger, R., & Barnes, R. 2015, AsBio, 15, 119
Luger, R., Sestovic, M., Kruse, E., et al. 2017, NatAs, 1, 0129
Massie, S. T., & Hunten, D. M. 1981, JGRC, 86, 9859
McElroy, M. B., Dak Sze, N., & Ling Yung, Y. 1973, JAtS, 30, 1437
McElroy, M. B., & Donahue, T. M. 1972, Sci, 177, 986
Meadows, V. S., Arney, G. N., Schwieterman, E. W., et al. 2018, AsBio, 18, 133
Misra, A., Meadows, V., Claire, M., & Crisp, D. 2014, AsBio, 14, 67
Nair, H., Allen, M., Anbar, A. D., Yung, Y. L., & Clancy, R. T. 1994, Icar, 111, 124
Papaloizou, J. C., Szuszkiewicz, E., & Terquem, C. 2017, MNRAS, 476, 5032
Rimmer, P. B., & Helling, C. 2016, ApJS, 224, 9
Roehl, C. M., Nizkorodov, S. A., Zhang, H., Blake, G. A., & Wennberg, P. O. 2002, JPCA, 106, 3766
Rugheimer, S., Kaltenegger, L., Segura, A., Linsky, J., & Mohanty, S. 2015, ApJ, 809, 57
Schumann, U., & Huntrieser, H. 2007, ACP, 7, 3823
Segura, A., Kasting, J. F., Meadows, V., et al. 2005, AsBio, 5, 706
Sen, B., Toon, G. C., Osterman, G. B., et al. 1998, JGRD, 103, 3571

Sleep, N. H., & Zahnle, K. 2001, JGRE, 106, 1373
Snellen, I. A., De Kok, R. J., De Mooij, E. J., & Albrecht, S. 2010, Natur, 465, 1049
Sullivan, P. W., Winn, J. N., Berta-Thompson, Z. K., et al. 2015, ApJ, 809, 77
Thalman, R., Zarzana, K. J., Tolbert, M. A., & Volkamer, R. 2014, JQSRT, 147, 171
Tian, F., France, K., Linsky, J. L., Mauas, P. J., & Vieytes, M. C. 2014, E&PSL, 385, 22
Tian, F., & Ida, S. 2015, NatGe, 8, 177
Turbet, M., Bolmont, E., Leconte, J., et al. 2018, A&A, 612, A86
Van Grootel, V., Fernandes, C. S., Gillon, M., et al. 2018, ApJ, 853, 30
Von Braun, K., Boyajian, T. S., van Belle, G. T., et al. 2014, MNRAS, 438, 2413
Walker, J. C., Hays, P. B., & Kasting, J. F. 1981, JGRC, 86, 9776
Wang, Z., Wang, W., Tham, Y. J., et al. 2017, ACP, 17, 12361
Wolf, E. T. 2017, ApJL, 839, L1, [Erratum: Wolf, E. T. 2018, ApJL, 855, L14]
Wong, M. L., Charnay, B. D., Gao, P., Yung, Y. L., & Russell, M. J. 2017, AsBio, 17, 975
Wordsworth, R., & Pierrehumbert, R. 2013, Sci, 339, 64
Youngblood, A., France, K., Loyd, R. P., et al. 2016, ApJ, 824, 101
Zhang, Z., Zhou, Y., Rackham, B. V., & Apai, D. 2018, AJ, 156, 178